Unifying Factory ESD Measurements and Component ESD Stress Testing

Julian A. Montoya and Timothy J. Maloney

Intel Corporation, RA1-220, Hillsboro, OR 97124

Intel Corporation, SC12-607, Santa Clara, CA 95052

(503) 613-9268; julian.a.montoya@intel.com

Abstract - ESD events are detected in the factory using an oscilloscope and a broadband E-field antenna for observing the radiation. These results are correlated to component CDM ESD test data for the first time. We show how the gap was bridged with factory data and laboratory observations of electric dipole radiation, with the peak-to-peak voltage swing (Vp-p) of the antenna signal proven to be a key parameter. We also formulate a circuit model of the standard CDM tester, and clearly show the influence of certain features. Finally, we use both factory and CDM test results in a statistical model for predicting factory ESD fallout in DPM.

I. Introduction

In recent years it has become common to use an antenna and oscilloscope to detect ESD in a manufacturing environment [1-2]. The method is easy to use and can distinguish an ESD event from other electromagnetic anomalies. But until now, no studies have related factory ESD event detection to component level ESD stress testing. In this work, we correlate factory level ESD event amplitudes, as measured with an antenna and oscilloscope, with stress voltages (and charge packets) used in modern charged device model (CDM) component stressing. The paper will also discuss stochastic methods that enable one to predict factory ESD fallout, given enough factory and component data.

The use of a wide bandwidth antenna and oscilloscope to detect ESD events has become the norm in recent years. The method can quickly and accurately identify sources of ESD, allowing the ESD specialist to make effective adjustments on the manufacturing line. But as we gained experience with this method, it was natural to ask, "What is the relation between the antenna and oscilloscope factory data to the component level ESD stress data?" After a significant effort across several organizations, the fundamental answers are clear. We also have a basic stochastic model that uses the accumulated factory and component data to predict ESD induced factory fallout. In order to reach these findings, we had to examine both the factory measurements and the CDM test equipment.

II. Detecting ESD with Antenna and Oscilloscope

A. Method

In the hands of a trained user in the factory, the broadband near-field antenna coupled with a high speed oscilloscope provides a low-cost, reliable means of detecting ESD and confirming ESD fixes. The concept is essentially to detect the electromagnetic radiation emitted by an ESD event, while distinguishing its electromagnetic (EM) signature from that of other EM anomalies in the environment. Figure 1 shows an E-field ball antenna (often used to detect EM interference or EMI) mounted near a component loader being monitored for ESD.

When an ESD event happens, the oscilloscope triggers and displays a waveform such as the one shown in Figure 2. The dampened sinusoid, which has fast rise time, ringing in the hundreds of MHz, and decay over perhaps 50-75 nanoseconds, becomes familiar to the operator as the ESD signature and is identified as such. We next asked why the ESD signature looks like this and what are its important figures of merit.

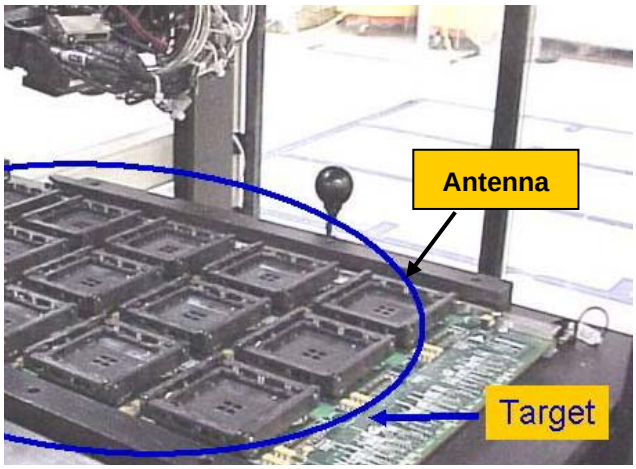

Figure 1. Ball antenna set up near a component loader for burn-in boards.

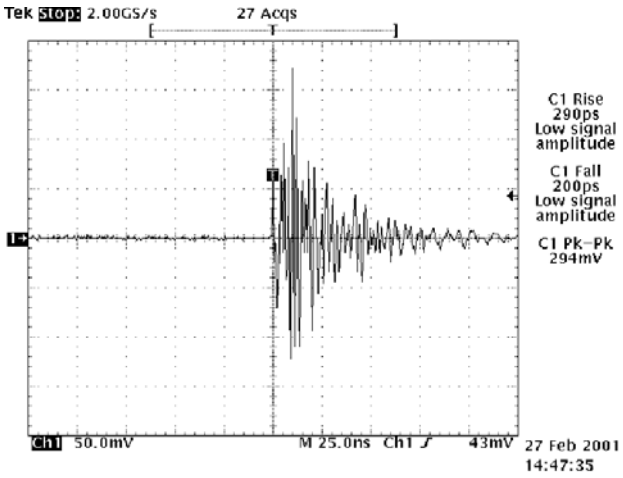

Figure 2. Typical waveform detected by ball antenna near component loader, showing ringing for 50-75 nanoseconds.

B. Lab Experiments

1. Dipole #1, FIM-CDM discharge

Lab experiments with a setup as shown in Figure 3, Dipole #1, were able to create CDM-like ESD events with a field-induced method (FIM) in a controlled way. A metal field plate on the top of the component, having a known voltage and capacitance to the ground plane, was employed. A pin extender forced the discharge to occur to a certain pin. The resulting waveform looked very much like the factory waveform in Fig. 2. While the CDM current passing through that pin can be shown (using a current probe) to be a unipolar impulse a few nanoseconds long, as indicated by the CDM test spec [3] and experimental studies going back many years [4], the radiated EMI is oscillatory, and lasts much longer, because of the oscillation of the ground plane. This is the only explanation for why the EMI lasts 50-75 nanoseconds. However, we find that the maximum peak-to-peak voltage swing Vp-p relates directly to the size of the main impulse, created by an electric dipole.

The main finding of the lab experiment is that regardless of component package size, the maximum EM pulse amplitude Vp-p is proportional to the charge packet associated with the specific ESD event. Thus at a given distance D, we measure roughly the same millivolts per nanocoulomb for different size packages, as shown in Figure 4, where Part 1 is about half the size Part 2 and the field-plate-to-ground capacitances are listed. We now have an idea of what kind of charge quantities are involved in the factory events, although there can be considerable variation in the efficiency of the radiator. The 300 mV/nC at 12" (30 cm) shown in Fig. 4 is fairly efficient, one reason for which is that the pin extender, about 1.2 cm (=Δz) long, creates a strong electric dipole $q_0\Delta z$. Let us briefly review electric dipole radiation before going further.

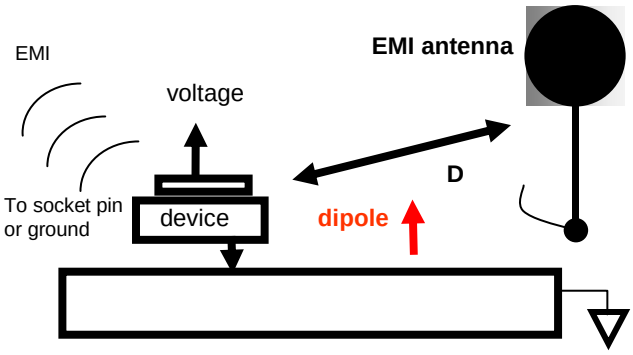

Figure 3. Dipole #1, field plate setup for creating radiated EMI due to CDM event with known charge packet.

2. Electric Dipole Radiation

Figure 5 shows an oscillating "Hertzian" electric dipole (a) and the (far field) radiation pattern (b) due to such a dipole. Note that the E-field is proportional to the dipole strength, i.e., the amount of charge q_0 times the separation Δz. As shown, the radiation is at a maximum when "broadside" of the dipole, where θ is the angle made with the dipole vector. These simple far field conditions are achieved at distance r when $\omega r/c >> 1$, so given that our CDM dipole is a short, broadband spike [4], there will be many frequencies; thus near and intermediate zone conditions will also apply [5].

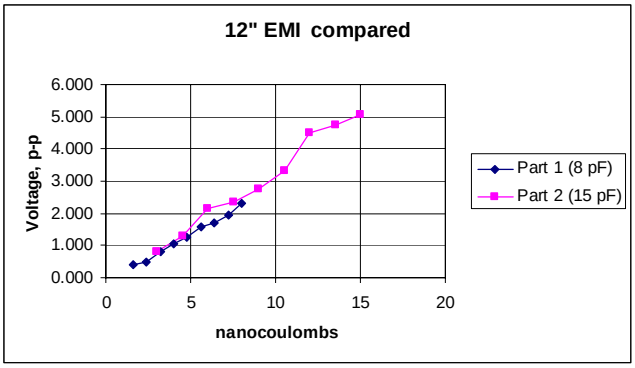

Figure 4. EMI, as measured by maximum Vp-p, as a function of CDM charge packet in nanocoulombs, for experiments as in Dipole #1, Fig. 3. Capacitance to ground of the field plates of the two components is measured with the pin extender in place.

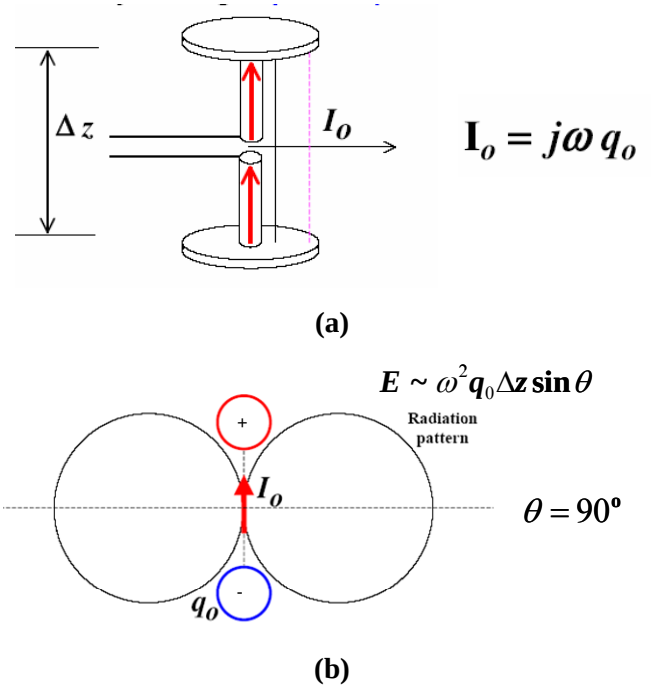

Figure 5. (a) Radiating electric dipole and (b) angular distribution and E-field of far-field radiation due to oscillating separated charge.

3. Dipole #2, Capacitor into Ground Plane

In order to understand more about EMI from discharging components as in the factory (Figs. 1 and 2) and the lab (Figs. 3 and 4), we built several artificial EMI zap creator units that mimic the radiative event of Fig. 2. Dipole #2 (Figure 6) was built out of printed circuit board material and discharges a 19 pF capacitor through a relay into an extended ground plane. It was expected to be an inefficient radiator and was indeed. Only about 120 mV/nC resulted as Vp-p for the ball antenna, under conditions similar to Fig. 3. But this kind of situation exists in the factory as well, and should be recognized because it results in larger estimates for the charge packet.

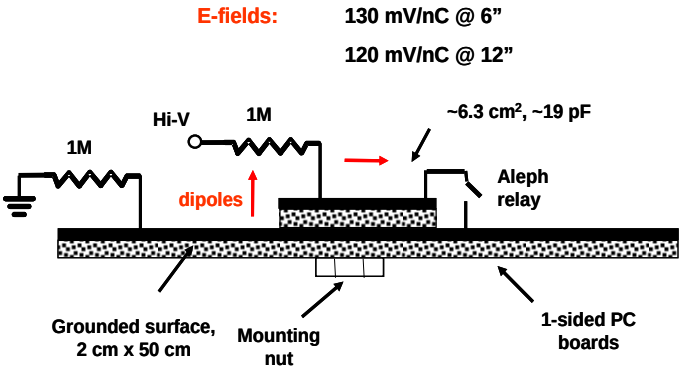

Figure 6. Dipole #2, built and tested to check EMI levels from a poor radiator.

4. Dipole #3, Folded Dipole Radiator

We also built a very efficient radiator for lab use, as shown in Figure 7. A 12.5 pF capacitor is discharged across wire inductance plus a small inductor, made from 1.9 cm of 300 ohm twin lead (about 20 nH), which drives a folded dipole antenna about 25-30 cm long. Waveforms again resemble Fig. 2 and ring for considerable time. The efficiency of this radiator in mV/nC is similar to the strong dipole of Fig 3. This radiator was built to be employed in a battery-operated package, complete with voltage supply, so that CDM-like EMI spikes could be created at will in the factory, for checkout of the antenna detection system.

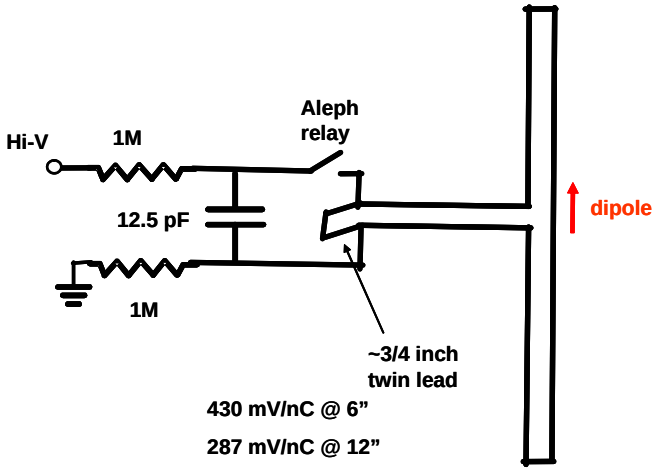

Figure 7. Efficient radiator, built to drive a folded dipole antenna and produce a pulse resembling factory EMI due to CDM.

5. Dipole #4, Non-Socketed CDM Tester Aperture

An obvious choice for observing EMI from a CDM discharge event is the familiar component nonsocketed CDM (ns-CDM) tester that we use to qualify parts. The CDM event created in these testers is confined to the inside of a metal box and is not easy to observe in the same way as factory events. But strong levels can still be observed in the case of the robotic CDM (RCDM) machine, due to a window above a 13.7 cm diameter circular aperture in a metal plate at the top of the machine. Figure 8 shows the configuration.

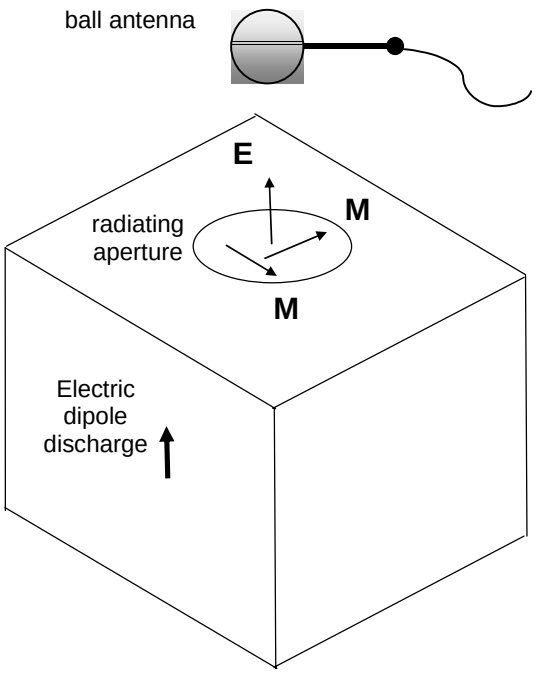

Figure 8. Discharge event inside non-socketed CDM machine creates radiation. Ball antenna is in position to pick up radiation from a 13.7 cm aperture at top of unit.

The detected EMI event (Figure 9) again lasts 50-75 nanoseconds, long after the discharge event, so clearly some ringing inside the box is taking place. The Vp-p, at 1.4V/nC, is stronger than for any of the other radiated events and shows what a strong oscillation is set up inside the box. Interpreting the EMI result is a good opportunity to apply small aperture theory [6,7] up to a few hundred MHz, where the wavelengths are on the order of a meter or more, and the aperture is "small" because ka>>1 ($k=2\pi/\lambda=\omega/c$, a the aperture radius).

Small aperture theory shows that the radiated fields are equivalent to radiation from a combination of electric and magnetic dipoles at the aperture, as seen in Fig. 8. These dipoles satisfy the electromagnetic boundary conditions of the aperture very nicely [6,7]. The electric dipole will be normal to the plane of the top deck and the magnetic dipole(s) will lie in that plane. Exact magnitudes depend on the incident radiation, which we expect to be pretty well randomized by the interior of the tester. We positioned the antenna at least 15 cm above the aperture in order to be in well behaved radiation zones [5] of the dipoles, and to avoid any complications due to being too close to the aperture plane [6,8].

To apply aperture theory to the spectrum seen in Fig. 9, one needs to know the spectral distribution of the radiation incident on the aperture, but even that is not clear. The radiation a large distance from a dipole source (far field) is a plane wave, having equal parts electric and magnetic field, and is the easiest case to analyze in terms of aperture theory. It is not known whether the radiation inside the box is equivalent to a plane wave, but there is a good case for substantial **E** and **H** components due to the obvious electric dipole and the current injection into the grounded walls through the sensing cable [3]. The **E** or **H** far field dipole radiation goes as ω^2 times the dipole moment [5], but we're not sure that relates to the radiation hitting the aperture—the latter may itself be in the near field of internal electric and magnetic sources at many wavelengths, and near-field radiation goes as lower powers (1 and 0) of ω. Even so, the aperture boundary conditions should again be satisfied by dipoles, whose radiated E-fields are then picked up by the antenna at a known distance. At r=15 cm from the aperture, $kr \approx 1$ at about 300 MHz or 1 meter wavelength, which happens to be the radiation peak for Fig. 9. This is in the intermediate zone, a thorough mix of near-field and far-field radiation from the dipoles [5].

What is the meaning of the 300 MHz peak, f_{max}? If the antenna signal is truly proportional to E-field, it is the maximum of a spectral function resulting from multiplying an (unknown) internal spectrum by a weighted sum of ω^0, ω^1 (near field) and ω^2 (far field) terms, depending on the mix of near and far field effects for each ω. Near field is known to be very important for 300 MHz and below, so Fig. 9 might be called the ω^1 spectrum. It can be compared to Figure 10, taken with antenna at 30 cm (12") above the aperture, where the radiation peak is at about 500 MHz. In that case, $kr \approx 3.14$ at f_{max} and there is a much heavier far-field (ω^2) contribution at that

frequency (as the near fields by comparison are down by 0.32 and 0.10 for ω^1 and ω^0 respectively), so this might be called the ω^2 spectrum.

Figure 9. Waveform (100 ns/div) and spectrum (200 MHz/div; 1GHz at middle, 20 db/div) for ns-CDM machine (Fig. 8) zap of 500 V, 2.5 nC charge packet, Vp-p of 3.5V, ball antenna 15 cm (6") above aperture.

Figure 10. Waveform (100 ns/div) and spectrum (200 MHz/div; 1GHz at middle, 20 db/div) for ns-CDM machine (Fig. 8) zap of 500 V, 2.5 nC charge packet, Vp-p of 882mV, ball antenna 30 cm (12") above aperture.

If the tailing part of the unknown internal spectrum is describable by a Gaussian (the Fourier Transform of a Gaussian CDM impulse in time) of $\exp(-\omega^2/\omega_0^2)$, then the maxima of the functions $F1= \omega\exp(-\omega^2/\omega_0^2)$ and $F2= \omega^2\exp(-\omega^2/\omega_0^2)$ can be compared. These are $\omega_0/\sqrt{2}$ and ω_0, respectively, giving a ratio of 0.707 for the maxima. The comparison to 0.6 (300 and 500 MHz in Figs. 9 and 10) is not bad given that the internal spectrum is largely unknown and that we have not accounted for the very near field ω^0 radiation, which goes as $1/(kr)^3$ and is important for the r=15 cm case, possibly lowering the measured f_{max}.

500 MHz for the f_{max} of the ω^2 spectrum is also consistent with a Gaussian spike of 1.27 nanosec width, about right for CDM. But this also means that the internal spectrum must be mostly undisturbed from the basic CDM current spike, which is consistent with the ringing of the ground metal around the aperture being the primary source of radiation.

The Vp-p of the EMI detected at 15 cm above the aperture of the ns-CDM machine also turns out to relate well to the charge packet, as shown in Figure 11 (charge packet is calculated as discussed in the next section). Part P was 31mm x 31 mm in area, delivering a substantial charge packet. For five different packages, having areas up to twice that of Part P, Vp-p was proportional to charge packet size, as seen earlier in Fig. 4.

With the antenna at 30 cm from the aperture, Vp-p also grew with Q as expected, but it fit a 2nd order polynomial curving upward, not a line. As yet, this is not explained.

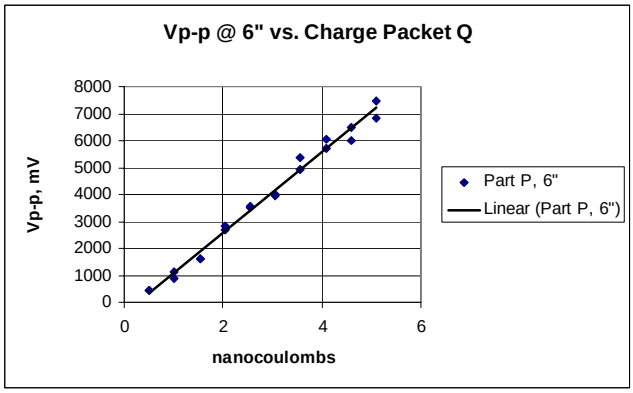

Figure 11. Vp-p vs. charge packet in nC; EMI antenna 15 cm (6") above aperture of ns-CDM machine. Voltages were 100-1000V for 9.6 cm2 package. Vp-p of 1.4V/nC results; very sensitive but linear.

C. Circuit Model of Nonsocketed CDM Tester

1. Field-Induced CDM Testing

Now that we recognize the importance of the basic 1-2 nanosecond charge packet of CDM [3,4], it is helpful to consider the immediate charge Q_{imm} that results from a non-socketed CDM tester as modeled in Figure 12. Cfrg is the capacitance from the top ground plane to the field plate. Cf is the capacitance of the component to the field plate, and Cg is the capacitance of the top ground plane to the component, both of which scale with component area. Their ratio

is Cg/Cf = $t_f/(\varepsilon_r t_g)$, where t_f is the dielectric thickness (fractions of a mm plus package dielectric), ε_r is the relative dielectric constant of the dielectric (usually 3 to 4), and t_g is the space from the top ground plate to the package metal, roughly the pogo pin length of 5-7mm. Thus Cg/Cf is a small number. The field plate, isolated from the voltage supply, is charged to Vf. When the pogo pin touches the pin under test, the switch is closed and (neglecting overshoot effects) the resulting charge packet is

$$Q_{imm} = Vf\left[\frac{Cf}{Cg+Cf}\right]\left[Cg + \frac{Cf * Cfrg}{Cf + Cfrg}\right] = Q_1 + Q_2 .$$

Usually, because of the thin dielectric, Cf far outweighs Cg and maybe even Cfrg. The top ground plane area is much larger than package area, so Q_2 can be much more than Q_1. This circuit model has been shown to agree very closely with the charge packet as measured by integrating waveforms observed through the 50-ohm cable attached to the 1-ohm disk resistor [3]. The resulting number of nanocoulombs in a CDM event of a given voltage (the charge packet) is thus very interesting to comprehend and compare with the expected factory events, now measured by antenna and oscilloscope. As discussed above, the EMI antenna should pick up a Vp-p signal proportional to the charge packet Q_{imm}. This model was used to calculate the charge packets for Figs. 9-11.

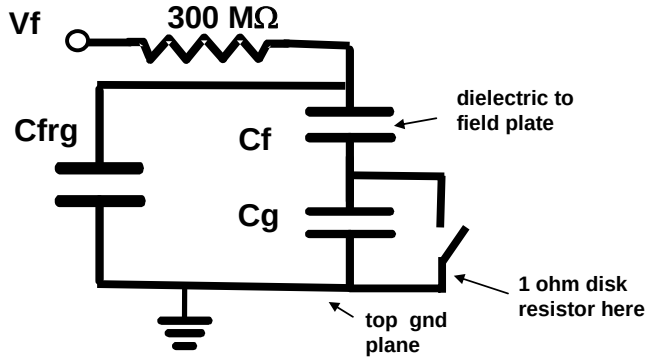

Figure 12. Circuit model for ns-CDM machine with component or test fixture in place. Switch closure happens when the pogo pin hits the component pin or test capacitor.

Notice in the expression for Q_{imm} that Cfrg, the plate capacitance unrelated to the component, has the effect of including more of Cf into Q_{imm} as the package area gets smaller. This is because as Cf becomes comparable to or smaller than Cfrg (about 4.3 pF), it is less reduced by Cfrg in the charge quantity Q2. So smaller-area packages suffer more charge per unit area (which is proportional to E-field) when tested at a given voltage.

2. Direct Charge CDM Testing

Direct charging is almost the same circuit model as Fig. 12 but not exactly. Figure 13 should be a good representation if the field plate is still grounded through high resistance. The charge packet Q_{imm} is nearly the same as the field-induced model, but there is no factor of $C_f/(C_g+C_f)$ in the expression, so direct charging adds a little more charge. To be exact, this is a factor of 1+Cg/Cf more charge, or $1 + t_f/(\varepsilon_r t_g)$, as discussed above, not usually much of an increase.

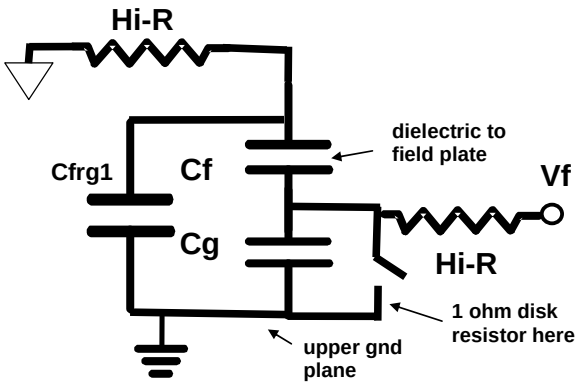

Figure 13. Circuit model of direct charge CDM test. Charge packet that flows through the switch immediately is Q_{imm} = Vf*(Cg + Cf*Cfrg/(Cf+Cfrg)), slightly more than for the field-induced model of Fig. 12.

The simple circuit models in Figs. 12 and 13 do not consider the influence of the 50-ohm cable connection from the top ground plate to the metal frame of the tester, but the shield of that cable carries the injected current to that frame and clearly influences the external radiation as discussed in Section B.5. We have also observed some "stray" pulses arriving back at the 1-ohm resistor, after the main CDM discharge, that appear to be related to this connection. This is a whole new topic that was opened up by these studies and will have to be discussed at a later time.

D. Factory EMI Data and Risk Assessment

EMI data for factory situations like Figure 1 are collected regularly as part of equipment qualification activities, and periodically thereafter. For one example of a 42.5 mm x 42.5 mm component in a 604-pin PGA package, here called Part D, we collected the EMI data in Figure 14, with the antenna 15-30 cm from the parts, much like Fig. 1. Fig. 14 shows how the Vp-p of the 45 recordable events were distributed, in bins of 22.5 mV width beginning at 25.5-48 mV and ending at 159.5-182 mV, with no

events observed above that level. Proper material selection as well as routine maintenance is expected to keep the EMI level low.

What is the meaning of the Vp-p data in Fig. 14? If Vp-p as measured with an antenna and oscilloscope truly is proportional to CDM charge packet, we can guess the charge packet given the observed range of Vp-p mV/nC as discussed above. We are most interested in low estimates for mV/nC, as with the poor radiators (~125 mV/nC), because they would result in the largest estimated charge packets. Seen in this way, the worst event observed for Part D (182 mV) would correspond to 1.46 nC for a poor radiator, and less than half that for a reasonably good radiator. Now turning to the Q_{imm} model in Section C, we find (using typical values of dielectric thickness and probe length) that the 604-pin PGA part (18.06 cm^2 in area) reaches a level of 1.46 nC at <250V. In this way we can know the range of CDM stresses that may be routinely inflicted on parts in the factory. Passing CDM tests to higher levels assures against "outlier" events that may not have been observed in the monitoring session.

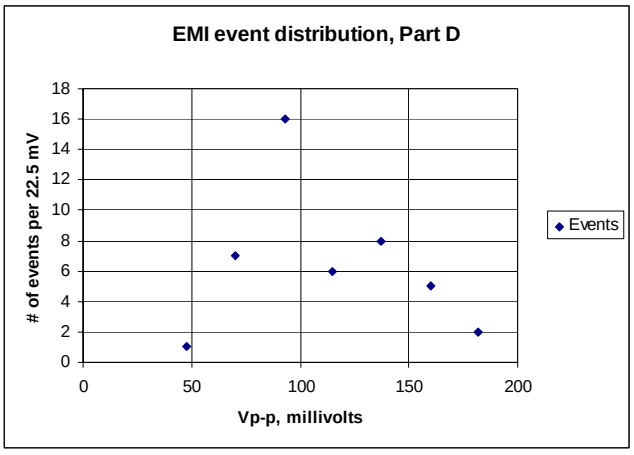

Figure 14. Bin count (22.5 mV bins ending at each plot point) of EMI events for a 604-pin PGA component in a loader, where Vp-p is believed proportional to CDM charge packet.

How do we quantify the risk once we have some idea of the factory stress (Fig. 14) and also know the CDM test results for the component? To examine that, we developed a stochastic model to predict component fallout. Details of the model are in Appendix A, but here is a brief summary. For a given component with m pins, the probability of destruction Δ can be found by knowing F(q), the probability that a factory event's charge packet is between the threshold of interest q_0 and q (Fig. 14 helps to know this); $\phi_1(k)$, the probability that pin k will be hit; and $\phi_2(q,k)$, essentially the component test data or probability that pin k will be killed by charge q. Integrating over all charge packets and summing over all pins, this relationship is

$$\int_{q_0}^{\infty} \frac{dF}{dq}\left[\sum_{k=1}^{m}\phi_1(k)\phi_2(q,k)\right]dq = \Delta.$$

Conventional statistical methods tell us that if we have *i* sub-processes and an event rate λ_i, time T_i and associated Δ_i for each, then the expected component level manufacturing fallout in defects per million (DPM) is expected to be

$$\boldsymbol{DPM}_{\boldsymbol{mfr}} = 10^6 \sum_{\boldsymbol{i}} \Delta_{\boldsymbol{i}} \lambda_{\boldsymbol{i}} \boldsymbol{T}_{\boldsymbol{i}}.$$

With this model, the factory antenna data, lab correlation, and CDM test data can all be merged to assess ESD risk to components in a highly rigorous way.

III. Discussion and Summary

This work has unified two substantial bodies of work in ESD, factory static monitoring with EMI ball antennas and ESD test data with the ns-CDM tester. We have studied radiating CDM-like electric dipoles of various kinds, including components constructed to radiate as if they were experiencing a factory event, and including the ns-CDM tester itself, to understand the character of the EMI event when caused by CDM ESD. We find that the EMI event lasts 50-75 nanoseconds, much longer than the 1-2 nanosecond CDM current spike through the component, but occurring because of ringing in the ground plane. We also have gained confidence in the utility of the peak-to-peak voltage (Vp-p) of the ESD EMI event as observed with the ball antenna, as it has consistently turned out to be proportional to the size of the CDM charge packet. But the efficiency of the particular dipole radiator can vary widely, leading to conservative estimates of the factory charge packet based on a possible "poor" radiator, delivering perhaps only 125 mV/nC. In the future, factory equipment could be subjected to measured amounts of CDM-like charge injection to gain confidence in a presumed level of mV/nC of Vp-p.

The ns-CDM component tester also produces observable, and recognizably CDM-like, EMI radiation, even though this has to be observed outside the cabinet where the test discharge takes place, above an aperture. The radiation is so strong that it appears that the ground metal inside the cabinet is ringing here in direct response to the charge injection, a kind of giant magnetic dipole to go with the obvious electric dipole in the discharge head. The spectrum of the observed radiation outside the aperture tends to support this as well. The observed Vp-p in the EMI

antenna near the machine aperture is proportional to CDM charge packet, again consistent with other observations. To calculate the ns-CDM machine's charge packet, we developed a circuit model for the ns-CDM tester and confirmed its accuracy with observed CDM waveforms. The circuit model helps the user understand how the dielectric above the field plate, the top ground plate, the component area, and other parameters influence the final charge packet. Formulating a circuit model also led us to recognize the influence of the discharge head's cable shield on the aperture radiation and on "stray" pulses arriving back at the discharge head, all of which is still being studied.

With some confidence in the relation between Vp-p EMI data and CDM charge packet Q_{imm}, we can begin to estimate the real risk to components in the factory environment. Factory EMI data and CDM test data can now be employed in a statistical model to estimate risk of component failure, ending in an estimate of defects per million (DPM). With continuous improvement of our knowledge of the probability functions, we can eliminate worst-case assumptions one by one and arrive at arrive at more realistic methods of managing ESD risk as technology advances.

Appendix A: Stochastic Model for ESD Risk Assessment

Definitions:

$P_1(n)$: probability that component X will suffer n CDM ESD events with charge packet $q>q_0$ during test and manufacturing as a packaged component. n=0,1,2,…; discrete distribution.

$\phi_1(k)$: conditional probability that pin k will be the victim of a CDM ESD event on component X, given that an event has occurred; component X has pins 1,…,m. Discrete distribution; k=1,2,3,…m.

F(q): probability that a CDM charge packet in an event happening to component X is less than q, nanocoulombs. Continuous distribution; $F(q_0)=0$, q_0 the threshold of interest.

$\phi_2(q,k)$: conditional probability that a CDM zap of charge packet q to pin k of component X will cause failure, given that event q has occurred. Continuous distribution in q; $\phi_2(q_0,k)=0$.

Notes: Remember to consider this for both + and – charge. Test data must be used to formulate ϕ_2, so any conflict between test failure and "real" CDM failure may be due to rise time. There may have to be a multiplier to be applied to the factory charge to get the charge needed to cause test failure.

Objective is to find the probability P_{mfr} that component X will go through the manufacturing line and fail. Then DPM = 10^6 x P_{mfr}.

Relationships:

Because $P_1(0)\geq 0$, $\sum_{i=1}^{\infty} P_1(i) \leq 1$.

$\sum_{i=1}^{\infty} iP_1(i)$ = average number of events happening to a given component X during manufacturing. If there is a rate λ at which CDM events $q>q_0$ happen to a given one of a collection of parts on the production line, we can deduce P_1 from the Poisson distribution, understanding that the parts are exposed for time T, so that $P_1(n) = e^{-\lambda T}\frac{(\lambda T)^n}{n!}$.

$\sum_{k=1}^{m} \phi_1(k) = 1$.

As above, $F(q_0)=0$. Also, $F(\infty)=1$. Define q_{av} such that $F(q_{av})=0.5$.

As above, $\phi_2(q_0,k)=0$. Also, $\phi_2(\infty,k)=1$. Define q_{kav} such that $\phi_2(q_{kav},k)=0.5$.

The Formula:

If a single event happens to a component, the probability of destruction is

$\int_{q_0}^{\infty} \frac{dF}{dq}\left[\sum_{k=1}^{m} \phi_1(k)\phi_2(q,k)\right]dq = \Delta.$ Thus the probability of survival of one event is $1-\Delta$, of two events is $(1-\Delta)^2$, etc.

For any $P_1(n)$, the probability of destruction of a single component going through the manufacturing line is thus

$P_{mfr} = \sum_{n=1}^{\infty} P_1(n) * (1-(1-\Delta)^n).$

For $P_1(n)$ obeying the Poisson distribution as above, the expression becomes

$$P_{mfr} = \sum_{n=1}^{\infty} P_1(n) * (1-(1-\Delta)^n)$$
$$= \sum_{n=1}^{\infty} e^{-\lambda T} * \frac{(\lambda T)^n}{n!} * (1-(1-\Delta)^n)$$
$$= 1 - e^{-\lambda T} - e^{-\lambda T} \sum_{n=1}^{\infty} \frac{[(\lambda T) * (1-\Delta)]^n}{n!}$$
$$= 1 - e^{-\lambda T} - e^{-\Delta\lambda T} + e^{-\lambda T} = 1 - e^{-\Delta\lambda T}.$$

Thus the probability of survival $P_{OK} = 1\text{-}P_{mfr} = e^{-\Delta\lambda T}$, and if there are a number of sub-processes in the production line, the final P_{OK} will be a product of exponentials with Δ_i, λ_i, and T_i appropriate to each sub-process. As long as the sum of $\Delta_i\lambda_i T_i$ products remains at a relatively low DPM level, the sum of products alone, $\sum_i \Delta_i \lambda_i T_i$, will suffice as an approximation of P_{mfr}.

Acknowledgments

The authors acknowledge the help of Intel statistician Curn Engelhard in the formulation of the stochastic model, and also acknowledge Calvin Hall's assistance in acquiring ns-CDM tester data. We also acknowledge the R&D and factory ESD engineers and technicians for their valuable data contributions.

References

[1] J. Bernier, G. Croft, and R. Rowther, "ESD Sources Pinpointed by Analysis of Radio Wave Emissions", 1997 EOS/ESD Symposium Proceedings, pp. 83-87.

[2] D.L. Lin, L.F. DeChiaro, and M.-C. Jon, "A Robust ESD Event Locator System with Event Characterization", 1997 EOS/ESD Symposium Proceedings, pp. 88-98.

[3] ANSI-ESDSTM5.3.1-1999, Charged Device Model (CDM)-Component Level Test Method, ESD Association, 1999.

[4] R. Renninger, "Methods of Charged-Device Model Electrostatic Discharges", 1991 EOS/ESD Symposium Proceedings, pp. 127-143.

[5] J. D. Jackson, *Classical Electrodynamics*, 3rd Edition (New York: John Wiley and Sons, 1999), pp. 410-413.

[6] H.A. Bethe, "Theory of Diffraction by Small Holes", Phys. Rev. 66, pp. 163-182 (1944).

[7] J.D. Jackson, *op. cit.*, pp. 422-425.

[8] S. Guha and G.D. Gillen, "Description of Light Propagation Through a Circular Aperture Using Nonparaxial Vector Diffraction Theory", Optics Express 13, 1424-1447 (2005). Available at http://www.opticsinfobase.org/abstract.cfm?id=82896.